Journal of Applied Analysis and Computation
Volume 5, Number 3, August 2015, 453–464
Website:http://jaac-online.com/
doi:10.11948/2015035

A HIGH ORDER CENTRAL-UPWIND SCHEME FOR HYPERBOLIC CONSERVATION LAWS*

Xiaohan Cheng[1], Yufeng Nie[1,†], Jianhu Feng[2] and Li Cai[1]

Abstract A high order central-upwind scheme for approximating hyperbolic conservation laws is proposed. This construction is based on the evaluation of the local propagation speeds of the discontinuities and Peer's fourth order non-oscillatory reconstruction. The presented scheme shares the simplicity of central schemes, namely no Riemann solvers are involved. Furthermore, it avoids alternating between two staggered grids, which is particularly a challenge for problems which involve complex geometries and boundary conditions. Numerical experiments demonstrate the high resolution and non-oscillatory properties of our scheme.

Keywords Hyperbolic conservation laws, central-upwind scheme, fourth order non-oscillatory reconstruction, high resolution.

MSC(2010) 65M08, 35L65.

1. Introduction

Systems of conservation laws are encountered frequently in science and engineering. With analytical solutions being unavailable in most cases, numerical method has become an indispensable tool in practical applications. Here, we are interested in Godunov-type methods which can be divided into two categories—upwind schemes and central schemes. For upwind schemes, solving Riemann problem at the discontinuous interfaces is required. Generally, this procedure is quite complicated and costly when solving systems of conservation laws. On the other hand, central schemes are based on averaging over Riemann fans. They require no Riemann solvers and therefore the complicated and time-consuming characteristic decomposition can be avoided. They are much simpler when compared with upwind schemes.

A general procedure used to obtain high order methods is based on high order piecewise polynomial reconstructions. Second order scheme utilized a piecewise linear reconstruction [13]. For third order scheme, Kurganov and Petrova proposed a piecewise non-oscillatory quadratic interpolant [9]. Alternatively, one can use the essentially non-oscillatory (ENO) reconstruction or its variants [1, 5, 11, 12, 15]. For example, CWENO reconstructions were introduced in the central framework to design central-upwind schemes for conservation laws or related problems [2, 4, 7].

†the corresponding author. Email address: yfnie@nwpu.edu.cn(Y. Nie)
[1]School of Science, Northwestern Polytechnical University, Xi'an 710129, China
[2]School of Science, Chang'an University, Xi'an 710064, China
*The authors were supported by National Natural Science Foundation of China (11471261,11171043) and the Doctorate Foundation of Northwestern Polytechnical University (CX201426).

However, ENO-type method employs smooth indicators. A certain a-priori information about the solution is needed and this may give rise to spurious oscillations or smearing near discontinuities [17]. To overcome this obstacle, one of the other strategies is to employ limiters to proceed the non-oscillatory polynomial reconstruction.

A new non-oscillatory reconstruction in one-dimension, which is fourth order accurate and avoids the computation of smooth indicators, was developed by Peer et al. [14]. The aim of this work is to present a non-staggered version of Peer's central scheme. Unlike the approach in [3], in which the reconstructed values of the staggered scheme are reaveraged, here we utilize the technique that is described in [8]. In this paper, we compute the widths of the Riemann fans by evaluating the local propagation speeds and present a semi-discrete form of fourth order central scheme. Without giving up simplicity, the resulting scheme is still free of Riemann solvers. What's more, it avoids the need to alternate between two staggered grids, which is particularly a challenge for practical problems with complex geometries and boundary conditions. The new scheme possesses an upwind nature since one-sided information is used to estimate the width of the Riemann fans. Thus, we also call it central-upwind scheme. It should be emphasized here that our scheme can avoid the calculation of smooth indicators and no a-priori information about the solution is needed when compared with the existing high order central-upwind schemes based on CWENO reconstruction. Such drawbacks of employing ENO-type reconstruction can be eliminated.

The rest of the paper is organized as follows. Section 2 describes the detailed procedure for designing our fourth order semi-discrete central-upwind scheme for solving one-dimensional problems. In section 3, we first give the central-upwind flux in two-dimensional case and then generalize the fourth order reconstruction to two-dimensional case. Finally, the proposed scheme is applied to solve a large class of test problems. Numerical results confirm the expected order of accuracy, high resolution and non-oscillatory properties of the scheme.

2. Fourth order central-upwind scheme

Consider hyperbolic systems of conservation laws in one spatial dimension,

$$u_t + f(u)_x = 0, \quad u(x, t = 0) = u_0(x), \tag{2.1}$$

where $u(x,t) = (u_1, \cdots, u_N)^T$ and $f(u) = (f_1, \cdots, f_N)^T$ are vectors of conservative variables and nonlinear fluxes respectively. For the sake of simplicity, the discretization is done on a uniformly spatial grid. Let $x_i = i\Delta x$, $x_{i\pm1/2} = (i \pm 1/2)\Delta x$, $i = 0, \ldots, NX$, where Δx is the cell size. Meanwhile let $t^n = n\Delta t$ and denote the sliding average of $u(\cdot, t)$ by $\bar{u}_i^n = \frac{1}{\Delta x}\int_{I_i} u(\xi, t^n)d\xi$ over the interval $I_i = (x_i - \frac{\Delta x}{2}, x_i + \frac{\Delta x}{2})$ at time $t = t^n$, we will show how to construct a new semi-discrete central-upwind scheme in the following.

2.1. Semi-discrete central-upwind scheme

Assuming we have known the cell-averages $\{\bar{u}_i^n\}$ at time $t = t^n$, the remained work is to obtain the cell-averages at the next time level t^{n+1}. From $\{\bar{u}_i^n\}$, we firstly

consider the following piecewise polynomial function interpolant,

$$u(x,t^n)=\sum_i R_i(x)\chi_i. \tag{2.2}$$

Here, χ_i denotes the characteristic function of the interval I_i, and $R_i(x)$ is a polynomial defined in I_i which should satisfy three requirements—accuracy, conservation and non-oscillatory. Unfortunately, $u(x,t^n)$ could be discontinuous at the cell interfaces $\{x_{i+1/2}\}$. We estimate the local propagation speeds of the discontinuities in the left- and right-direction by

$$a^-_{i+1/2}=\min_{u\in C(u^-_{i+1/2},u^+_{i+1/2})}\left\{\lambda_1\left(\frac{\partial f}{\partial u}(u)\right),0\right\}$$

and

$$a^+_{i+1/2}=\max_{u\in C(u^-_{i+1/2},u^+_{i+1/2})}\left\{\lambda_N\left(\frac{\partial f}{\partial u}(u)\right),0\right\},$$

respectively. Here, $\lambda_1<\cdots<\lambda_N$ represent the eigenvalues of the Jacobian $\frac{\partial f}{\partial u}$. $u^-_{i+1/2}=R_i(x_{i+1/2})$ and $u^+_{i+1/2}=R_{i+1}(x_{i+1/2})$ are the corresponding values of $u(x,t^n)$ at the cell interfaces $\{x=x_{i+1/2}\}$ and $C(u^-_{i+1/2},u^+_{i+1/2})$ is the curve in the phase space that connects $u^-_{i+1/2}$ and $u^+_{i+1/2}$ via the Riemann fan.

Next, we define two nonequal control volumes

$$[x^n_{i+1/2,l},x^n_{i+1/2,r}]\times[t^n,t^{n+1}]\quad\text{and}\quad[x^n_{i-1/2,r},x^n_{i+1/2,l}]\times[t^n,t^{n+1}],$$

with $x^n_{i+1/2,l}=x_{i+1/2}+\Delta t a^-_{i+1/2}$ and $x^n_{i+1/2,r}=x_{i+1/2}+\Delta t a^+_{i+1/2}$. Due to the finite speeds of propagation, the solution of (2.1) may be nonsmooth only inside the interval $[x^n_{i+1/2,l},x^n_{i+1/2,r}]$ for $t\in[t^n,t^{n+1}]$. Then integrating (2.1) directly over the above control volumes, we obtain the cell averages

$$\begin{aligned}\bar w^{n+1}_{i+1/2}=&\frac{1}{x^n_{i+1/2,r}-x^n_{i+1/2,l}}\left[\int_{x^n_{i+1/2,l}}^{x^n_{i+1/2}}R^n_i(x)dx+\int_{x^n_{i+1/2}}^{x^n_{i+1/2,r}}R^n_{i+1}(x)dx\right.\\&\left.-\int_{t^n}^{t^{n+1}}\Big(f(u(x^n_{i+1/2,r},t))-f(u(x^n_{i+1/2,l},t))\Big)\,dt\right]\end{aligned} \tag{2.3}$$

and

$$\begin{aligned}\bar w^{n+1}_{i}=&\frac{1}{x^n_{i+1/2,l}-x^n_{i-1/2,r}}\left[\int_{x^n_{i-1/2,r}}^{x^n_{i+1/2,l}}R^n_i(x)dx\right.\\&\left.-\int_{t^n}^{t^{n+1}}\Big(f(u(x^n_{i+1/2,l},t))-f(u(x^n_{i-1/2,r},t))\Big)\,dt\right].\end{aligned} \tag{2.4}$$

Finally, from these obtained values $\{\bar w^{n+1}_{i+1/2},\bar w^{n+1}_i\}$, we employ the same reconstruction of $u(x,t^n)$ which takes the form:

$$\widetilde w^{n+1}(x)=\sum_i\Big(\widetilde w^{n+1}_{i+1/2}(x)\chi_{[x^n_{i+1/2,l},x^n_{i+1/2,r}]}+\widetilde w^{n+1}_i(x)\chi_{[x^n_{i-1/2,r},x^n_{i+1/2,l}]}\Big). \tag{2.5}$$

Here, $\{\widetilde{w}_{i+1/2}^{n+1}(x), \widetilde{w}_i^{n+1}(x)\}$ and the χ's are the piecewise polynomial functions and the characteristic functions on the corresponding intervals, respectively. Projecting $\widetilde{w}^{n+1}$ back onto the cell I_i, we have

$$\begin{aligned}\bar{u}_i^{n+1} =& \frac{1}{\Delta x}\int_{x_{i-1/2}^n}^{x_{i+1/2}^n} \widetilde{w}^{n+1}(x)dx = \frac{1}{\Delta x}\Big[\int_{x_{i-1/2}^n}^{x_{i-1/2,r}^n} \widetilde{w}_{i-1/2}^{n+1}(x)dx \\ &+ \int_{x_{i-1/2,r}^n}^{x_{i+1/2,l}^n} \widetilde{w}_i^{n+1}(x)dx + \int_{x_{i+1/2,l}^n}^{x_{i+1/2}^n} \widetilde{w}_{i+1/2}^{n+1}(x)dx\Big].\end{aligned} \tag{2.6}$$

The above formula gives a fully discrete form of central-upwind scheme. With the help of Eq.(2.6), the semi-discrete approximation can be obtained by computing the derivative of $\bar{u}_i(t)$ with respect to t, namely

$$\frac{d}{dt}\bar{u}_i(t) = \lim_{\Delta t\to 0}\frac{\bar{u}_i^{n+1}-\bar{u}_i^n}{\Delta t} = \lim_{\Delta t\to 0}\frac{1}{\Delta t}\left[\frac{1}{\Delta x}\int_{x_{i-1/2}}^{x_{i+1/2}} \widetilde{w}^{n+1}(x)dx - \bar{u}_i^n\right]. \tag{2.7}$$

Now suppose that the slopes of $\widetilde{w}_{i\pm1/2}^{n+1}$ are uniformly bounded. Since the Riemann fans' widths take an upper bound of $(a_{i+1/2}^+ - a_{i+1/2}^-)\Delta t$, we find

$$\widetilde{w}_{i\pm1/2}^{n+1} = \bar{w}_{i\pm1/2}^{n+1} + O(\Delta t) \quad \forall x \in [x_{i\pm1/2,l}^n, x_{i\pm1/2,r}^n]. \tag{2.8}$$

Using the conservation property of the reconstruction we can have

$$\frac{1}{x_{i+1/2,l}^n - x_{i-1/2,r}^n}\int_{x_{i-1/2,r}^n}^{x_{i+1/2,l}^n} \widetilde{w}_i^{n+1}(x)dx = \bar{w}_i^{n+1}. \tag{2.9}$$

From (2.7)—(2.9) and the definition of $x_{i-1/2,r}^n$ and $x_{i+1/2,l}^n$, we obtain

$$\begin{aligned}\frac{d}{dt}\bar{u}_i(t) =& \frac{a_{i-1/2}^+}{\Delta x}\lim_{\Delta t\to 0}\bar{w}_{i-1/2}^{n+1} - \frac{a_{i+1/2}^-}{\Delta x}\lim_{\Delta t\to 0}\bar{w}_{i+1/2}^{n+1} \\ &+ \lim_{\Delta t\to 0}\frac{1}{\Delta t}\left(\frac{x_{i+1/2,l}^n - x_{i-1/2,r}^n}{\Delta x}\bar{w}_i^{n+1} - \bar{u}_i^n\right).\end{aligned} \tag{2.10}$$

Note that

$$\begin{aligned}&\lim_{\Delta t\to 0}\frac{1}{\Delta t}\left(\frac{x_{i+1/2,l}^n - x_{i-1/2,r}^n}{\Delta x}\bar{w}_i^{n+1} - \bar{u}_i^n\right) = \\ &\frac{a_{i+1/2}^- u_{i+1/2}^- - a_{i-1/2}^+ u_{i-1/2}^+}{\Delta x} - \frac{f(u_{i+1/2}^-) - f(u_{i-1/2}^+)}{\Delta x}\end{aligned} \tag{2.11}$$

and

$$\lim_{\Delta t\to 0}\bar{w}_{i+1/2}^{n+1} = \frac{a_{i+1/2}^+ u_{i+1/2}^+ - a_{i+1/2}^- u_{i+1/2}^-}{a_{i+1/2}^+ - a_{i+1/2}^-} - \frac{f(u_{i+1/2}^+) - f(u_{i+1/2}^-)}{a_{i+1/2}^+ - a_{i+1/2}^-}, \tag{2.12}$$

we can cast the semi-discrete scheme into the conservative form:

$$\frac{d}{dt}\bar{u}_i(t) = -\frac{H_{i+1/2}(t) - H_{i-1/2}(t)}{\Delta x} \tag{2.13}$$

with the numerical flux $H_{i+1/2}(t)$ expressed by

$$H_{i+1/2}(t) = \frac{a^+_{i+1/2} f(u^-_{i+1/2}) - a^-_{i+1/2} f(u^+_{i+1/2})}{a^+_{i+1/2} - a^-_{i+1/2}} + \frac{a^+_{i+1/2} a^-_{i+1/2}}{a^+_{i+1/2} - a^-_{i+1/2}} \left(u^+_{i+1/2} - u^-_{i+1/2} \right). \tag{2.14}$$

Here, we omit the trivial derivation. For more details, one can consult Kurganov's literature [8]. It should be realized that the resulting scheme's space order depends on the accuracy of the reconstructed $u(x, t^n)$ in (2.2).

2.2. Fourth order non-oscillatory reconstruction

In this subsection, we briefly describe the fourth order non-oscillatory reconstruction. Let us introduce some notation: $\Delta\bar{u}_{i+1/2} = \bar{u}_{i+1} - \bar{u}_i$, $\Delta^2\bar{u}_i = \bar{u}_{i+1} - 2\bar{u}_i + \bar{u}_{i-1}$, $\Delta^3\bar{u}_{i+1/2} = \Delta^2\bar{u}_{i+1} - \Delta^2\bar{u}_i$. In every cell I_i, we choose a degree-three polynomial reconstruction

$$R_i(x) = u^n_i + u'_i(\frac{x - x_i}{\Delta x}) + \frac{1}{2!}u''_i(\frac{x - x_i}{\Delta x})^2 + \frac{1}{3!}u'''_i(\frac{x - x_i}{\Delta x})^3. \tag{2.15}$$

Conservation requires $\frac{1}{\Delta x}\int_{I_i} R_i(x)dx = \bar{u}^n_i$, which, in turn, results with

$$u^n_i = \bar{u}^n_i - \frac{u''_i}{24}. \tag{2.16}$$

To achieve fourth order accuracy, the numerical derivatives $\frac{1}{\Delta x}u'_i$, $\frac{1}{(\Delta x)^2}u''_i$ and $\frac{1}{(\Delta x)^3}u'''_i$ must satisfy

$$\frac{1}{\Delta x}u'_i = \frac{\partial}{\partial x}u(x = x_i, t^n) + O(\Delta x)^3, \tag{2.17}$$

$$\frac{1}{(\Delta x)^2}u''_i = \frac{\partial^2}{\partial x^2}u(x = x_i, t^n) + O(\Delta x)^2, \tag{2.18}$$

$$\frac{1}{(\Delta x)^3}u'''_i = \frac{\partial^3}{\partial x^3}u(x = x_i, t^n) + O(\Delta x). \tag{2.19}$$

Apart from this, the reconstruction here should satisfy the non-oscillatory property under the meaning of WENO reconstruction.

Concluding the above requirements, u'_i, u''_i and u'''_i are stated as follows:

$$\begin{aligned} u'_i = &\mathbf{MM}\big(\Delta\bar{u}_{i-1/2} + \frac{1}{2}\mathbf{MM}(\Delta^2\bar{u}_{i-1} + \frac{7}{12}u'''_{i-1}, \Delta^2\bar{u}_i - \frac{5}{12}u'''_i), \\ &\Delta\bar{u}_{i+1/2} - \frac{1}{2}\mathbf{MM}(\Delta^2\bar{u}_i + \frac{5}{12}u'''_i, \Delta^2\bar{u}_{i+1} - \frac{7}{12}u'''_{i+1})\big), \end{aligned} \tag{2.20}$$

$$u''_i = \mathbf{MM}\big(\Delta^2\bar{u}^n_{i-1} + u'''_{i-1}, \Delta^2\bar{u}^n_i, \Delta^2\bar{u}^n_{i+1} - u'''_{i+1}\big), \tag{2.21}$$

$$u'''_i = \mathbf{MM}\big(\Delta^3\bar{u}_{i-1/2}, \Delta^3\bar{u}_{i+1/2}\big), \tag{2.22}$$

where the **MM** limiter can be expressed as

$$\mathbf{MM}(x_1, x_2, \cdots) = \begin{cases} \max_q\{x_q\}, & \text{if } x_q < 0 \ (\forall q), \\ \min_q\{x_q\}, & \text{if } x_q > 0 \ (\forall q), \\ 0, & \text{otherwise.} \end{cases} \tag{2.23}$$

3. Multidimensional extensions

The presented scheme in section 2 can be extended to several space dimensions easily. Without loss of generality, we now consider the two-dimensional (2-D) hyperbolic conservation laws,

$$u_t + f(u)_x + g(u)_y = 0. \tag{3.1}$$

For the same purpose of simplicity, both space and time discretizations of (3.1) are done on uniformly grids. We use the notation $(x_i, y_j) = (i\Delta x, j\Delta y)$ for the grid points and $\bar{u}^n_{i,j} = \frac{1}{\Delta x \Delta y}\iint_{C_{i,j}} u(x, y, t^n)dxdy$ for the cell averages on $C_{i,j} = [x_{i-1/2}, x_{i+1/2}] \times [y_{j-1/2}, y_{j+1/2}]$ at time $t = t^n$. Following the 'dimension-by-dimension' approach, the extension of our fourth order semi-discrete scheme for (3.1) is

$$\frac{d}{dt}\bar{u}_{i,j}(t) = -\frac{H^x_{i+1/2,j}(t) - H^x_{i-1/2,j}(t)}{\Delta x} - \frac{H^y_{i,j+1/2}(t) - H^y_{i,j-1/2}(t)}{\Delta y}, \tag{3.2}$$

where $H^x_{i+1/2,j}(t)$ and $H^y_{i,j+1/2}(t)$ are $x-$ and $y-$direction numerical fluxes, respectively,

$$\begin{aligned} H^x_{i+1/2,j}(t) =& \frac{a^+_{i+1/2,j} f(u^-_{i+1/2,j}) - a^-_{i+1/2,j} f(u^+_{i+1/2,j})}{a^+_{i+1/2,j} - a^-_{i+1/2,j}} \\ &+ \frac{a^+_{i+1/2,j} a^-_{i+1/2,j}}{a^+_{i+1/2,j} - a^-_{i+1/2,j}} \left(u^+_{i+1/2,j} - u^-_{i+1/2,j}\right), \\ H^y_{i,j+1/2}(t) =& \frac{b^+_{i,j+1/2} g(u^-_{i,j+1/2}) - b^-_{i,j+1/2} g(u^+_{i,j+1/2})}{b^+_{i,j+1/2} - b^-_{i,j+1/2}} \\ &+ \frac{b^+_{i,j+1/2} b^-_{i,j+1/2}}{b^+_{i,j+1/2} - b^-_{i,j+1/2}} \left(u^+_{i,j+1/2} - u^-_{i,j+1/2}\right). \end{aligned} \tag{3.3}$$

In practice, we may use

$$\begin{aligned} a^-_{i+1/2,j} &= \min\left\{\lambda_1\left(\frac{\partial f}{\partial u}\left(u^-_{i+1/2,j}\right)\right), \lambda_1\left(\frac{\partial f}{\partial u}\left(u^+_{i+1/2,j}\right)\right), 0\right\}, \\ a^+_{i+1/2,j} &= \max\left\{\lambda_N\left(\frac{\partial f}{\partial u}\left(u^-_{i+1/2,j}\right)\right), \lambda_N\left(\frac{\partial f}{\partial u}\left(u^+_{i+1/2,j}\right)\right), 0\right\}, \\ b^-_{i,j+1/2} &= \min\left\{\lambda_1\left(\frac{\partial g}{\partial u}\left(u^-_{i,j+1/2}\right)\right), \lambda_1\left(\frac{\partial g}{\partial u}\left(u^+_{i,j+1/2}\right)\right), 0\right\}, \\ b^+_{i,j+1/2} &= \max\left\{\lambda_N\left(\frac{\partial g}{\partial u}\left(u^-_{i,j+1/2}\right)\right), \lambda_N\left(\frac{\partial g}{\partial u}\left(u^+_{i,j+1/2}\right)\right), 0\right\} \end{aligned}$$

to estimate the local speeds. Here, $\lambda_1 < \cdots < \lambda_N$ denote the N eigenvalues of the Jacobian $\frac{\partial f}{\partial u}$ or $\frac{\partial g}{\partial u}$. The values at the cell interfaces are defined by $u^\pm_{i+1/2,j} = R_{i+1/2\pm1/2,j}(x_{i+1/2}, y_j)$ and $u^\pm_{i,j+1/2} = R_{i,j+1/2\pm1/2}(x_i, y_{j+1/2})$, which are obtained from the reconstructed polynomial $R_{i,j}(x, y)$.

Now, we generalize Peer's reconstruction to the 2-D case. Similar to the 1-D

case, the polynomial reconstruction is chosen of the form

$$\begin{aligned} R_{i,j}(x,y) =& u^n_{i,j} + u'_{i,j}\Big(\frac{x-x_i}{\Delta x}\Big) + u^{\backslash}_{i,j}\Big(\frac{y-y_j}{\Delta y}\Big) \\ &+ \frac{1}{2!}\left(u''_{i,j}\Big(\frac{x-x_i}{\Delta x}\Big)^2 + 2u^{\wedge}_{i,j}\Big(\frac{x-x_i}{\Delta x}\Big)\Big(\frac{y-y_j}{\Delta y}\Big) + u^{\backslash\backslash}_{i,j}\Big(\frac{y-y_j}{\Delta y}\Big)^2\right) \\ &+ \frac{1}{3!}\left(u'''_{i,j}\Big(\frac{x-x_i}{\Delta x}\Big)^3 + u^{\backslash\backslash\backslash}_{i,j}\Big(\frac{y-y_j}{\Delta y}\Big)^3\right) \\ &+ \frac{1}{3!}\left(3u^{\prime\wedge}_{i,j}\Big(\frac{x-x_i}{\Delta x}\Big)^2\Big(\frac{y-y_j}{\Delta y}\Big) + 3u^{\wedge\backslash}_{i,j}\Big(\frac{x-x_i}{\Delta x}\Big)\Big(\frac{y-y_j}{\Delta y}\Big)^2\right). \end{aligned} \tag{3.4}$$

Actually, we only need to know $R_{i,j}(x, y = y_j)$ and $R_{i,j}(x = x_i, y)$. Thus, $R_{i,j}(x, y)$ reduces to

$$R_{i,j}(x, y = y_j) = u^n_{i,j} + u'_{i,j}\Big(\frac{x-x_i}{\Delta x}\Big) + \frac{1}{2!}u''_{i,j}\Big(\frac{x-x_i}{\Delta x}\Big)^2 + \frac{1}{3!}u'''_{i,j}\Big(\frac{x-x_i}{\Delta x}\Big)^3 \tag{3.5}$$

and

$$R_{i,j}(x = x_i, y) = u^n_{i,j} + u^{\backslash}_{i,j}\Big(\frac{y-y_j}{\Delta y}\Big) + \frac{1}{2!}u^{\backslash\backslash}_{i,j}\Big(\frac{y-y_j}{\Delta y}\Big)^2 + \frac{1}{3!}u^{\backslash\backslash\backslash}_{i,j}\Big(\frac{y-y_j}{\Delta y}\Big)^3 \tag{3.6}$$

with $u^n_{i,j} = \bar{u}^n_{i,j} - \frac{u''_{i,j}+u^{\backslash\backslash}_{i,j}}{24}$. Therefore, we can carry out the computation of the coefficients $u'_{i,j}$, $u^{\backslash}_{i,j}$, $u''_{i,j}$, $u^{\backslash\backslash}_{i,j}$, $u'''_{i,j}$ and $u^{\backslash\backslash\backslash}_{i,j}$ in a similar way like (2.20)-(2.22). For example, $u'''_{i,j} = \mathbf{MM}(\Delta^3\bar{u}_{i-1/2,j}, \Delta^3\bar{u}_{i+1/2,j})$, $u^{\backslash\backslash\backslash}_{i,j} = \mathbf{MM}(\Delta^3\bar{u}_{i,j-1/2}, \Delta^3\bar{u}_{i,j+1/2})$, etc.

4. Numerical examples

In this section, a number of numerical examples are provided to illustrate the potential of the proposed scheme, which is abbreviated by SD4. To make a comparison, we present the results computed by the scheme from [3], which is also a non-staggered version of Peer's central scheme (we call it CNO4-N). For central-upwind scheme, we assume that the discontinuities can not arrive at the cell interfaces in a small time interval. Therefore, the CFL number should be chosen smaller than 0.5 to keep the scheme's stability. All cases are run with a CFL number of 0.3 and we march in time using a fourth-order explicit Runge-Kutta method, which is given by

$$\begin{aligned} k_1 &= L(u^n), \\ k_2 &= L(u^n + \frac{\Delta t}{2}k_1), \\ k_3 &= L(u^n + \frac{\Delta t}{2}k_2), \\ k_4 &= L(u^n + \Delta t k_3), \\ u^{n+1} &= u^n + \frac{\Delta t}{6}(k_1 + 2k_2 + 2k_3 + k_4), \end{aligned} \tag{4.1}$$

where the operator L in (4.1) represents the right-hand side of (2.13) or (3.2).

4.1. Assessment of accuracy

To test the accuracy, let us consider the transport equation $u_t + u_x = 0$ with the initial data $u(x, t = 0) = \sin(\pi x)$ on the interval $[-1, 1]$. The solutions are computed on different grids up to time $T = 10$. The time step Δt is chosen to be $\Delta x \times CFL$. We displayed the L^1- and L^∞-errors and the corresponding convergence rate in Table 1, respectively. It is noticed that both SD4 and CNO4-N can achieve fourth order accuracy in L^1 norm as the grids are refined. In L^∞ norm, both schemes can't achieve the desired accuracy. This is mainly due to the fact that the non-smooth limiters employed in the reconstruction lack regularity and make the scheme less accurate [16]. We can also observe SD4 gives errors of smaller magnitude and less computational time as compared with CNO4-N.

Table 1. Accuracy test for $u_t + u_x = 0$ with $u(x, t = 0) = sin(\pi x)$

Method	NX	L^1 error	L^1 order	L^∞ error	L^∞ order	Time(s)
SD4	40	2.242 e-3	-	2.951 e-3	-	2.367
	80	1.603 e-4	3.806	3.375 e-4	3.128	9.065
	160	1.133 e-5	3.823	3.782 e-5	3.158	35.30
	320	7.773 e-7	3.866	4.197 e-6	3.172	136.8
	640	5.193 e-8	3.904	4.634 e-7	3.179	978.8
CNO4-N	40	3.582 e-3	-	4.288 e-3	-	2.876
	80	2.417 e-4	3.889	4.847 e-4	3.145	10.93
	160	1.701 e-5	3.829	5.386 e-5	3.170	42.88
	320	1.176 e-6	3.854	5.954 e-6	3.177	170.7
	640	7.879 e-8	3.899	6.563 e-7	3.181	1030.1

4.2. Systems of conservation laws

Here, the proposed scheme is applied to the Euler equations of gas dynamics for an ideal gas with $\gamma = 1.4$,

$$\frac{\partial}{\partial t}\begin{pmatrix}\rho\\ \rho u\\ E\end{pmatrix} + \frac{\partial}{\partial x}\begin{pmatrix}\rho u\\ \rho u^2 + p\\ (E+p)u\end{pmatrix} = 0, \quad E = \frac{1}{2}\rho u^2 + \frac{p}{\gamma - 1}, \tag{4.2}$$

where the variables ρ, u, p and E denote the density, velocity, pressure and total energy, respectively. We will solve the following three different test problems which are commonly used by researchers. Here, the time step Δt is determined by

$$\Delta t = \frac{\Delta x \times CFL}{\max_i(c_i + |u_i|)}$$

with the local sound speed $c_i = \sqrt{\gamma p_i/\rho_i}$.

Sod's shock tube problem. We solve Eq. (4.2) with the initial data

$$\begin{pmatrix}\rho\\ u\\ p\end{pmatrix} = \begin{cases}(1, 0, 1)^T, & -0.5 \le x < 0,\\ (0.125, 0, 0.1)^T, & 0 \le x \le 0.5.\end{cases}$$

This initial discontinuity evolves into a left-going rarefaction wave, a right-going shock wave and a right-going contact discontinuity. We compute the solution at time $T = 0.16$. Comparing the results in Fig.1, we notice that both SD4 and CNO4-N resolve all the waves correctly. But, SD4 gives slightly higher resolution.

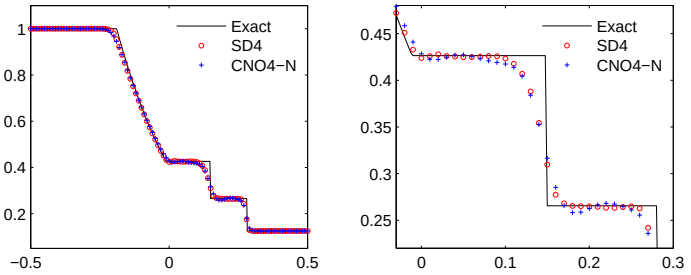

(a) Density (b) Zoomed region of density

Figure 1. Density of Sod's shock tube problem with NX=100

Lax's shock tube problem. We consider another initial data

$$\begin{pmatrix} \rho \\ u \\ p \end{pmatrix} = \begin{cases} (0.445, 0.698, 3.528)^T, & -0.5 \le x < 0, \\ (0.5, 0, 0.571)^T, & 0 \le x \le 0.5. \end{cases}$$

This is a more severe shock tube problem and oscillation may appear near discontinuities. Fig.2 shows the approximations to density at $T = 0.16$. As expected, we observe that there are slight oscillations near discontinuities for both schemes. However, SD4 is still less oscillatory than CNO4-N between the contact discontinuity and the shock.

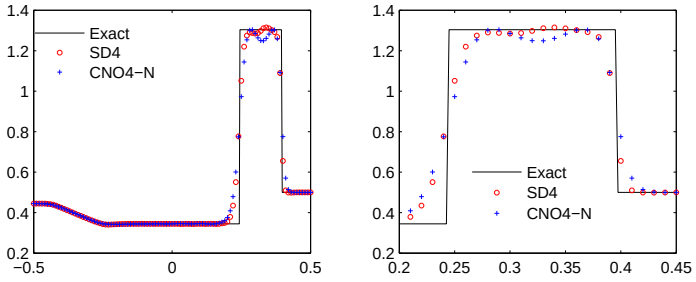

(a) Density (b) Zoomed region of density

Figure 2. Density of Lax's shock tube problem with NX=100

Shock-entropy problem. Here, we consider the following initial data

$$\begin{pmatrix} \rho \\ u \\ p \end{pmatrix} = \begin{cases} (3.857134, 2.629369, 10.33333)^T, & -5 \le x < -4, \\ (1 + 0.2\sin(5x), 0, 1)^T, & -4 \le x \le 5. \end{cases}$$

This problem describes a moving Mach 3 shock interacting with sine waves in density. Here, the computation is performed up to time $T = 1.8$ and the reference

solution is computed by WENO5 scheme [6] on a mesh of 5001 grid points. We present the results in Fig.3. For this problem, one can easily observe that the approximation of SD4 is more accurate than CNO4-N in sine wave regions.

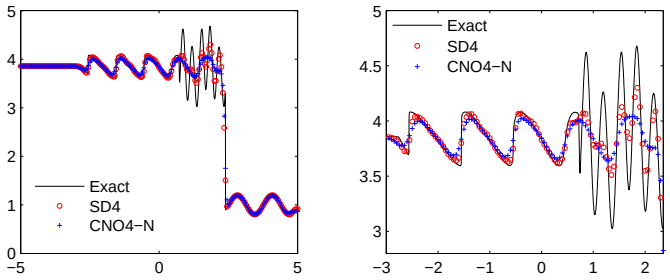

(a) Density (b) Zoomed region of density

Figure 3. Density of shock-entropy problem with NX=200

4.3. Riemann problems for two-dimensional Euler equations

Finally, let us consider the 2-D Euler equations of gas dynamics for an ideal gas with $\gamma = 1.4$,

$$\frac{\partial}{\partial t}\begin{pmatrix}\rho\\ \rho u\\ \rho v\\ E\end{pmatrix}+\frac{\partial}{\partial x}\begin{pmatrix}\rho u\\ \rho u^2+p\\ \rho uv\\ (E+p)u\end{pmatrix}+\frac{\partial}{\partial y}\begin{pmatrix}\rho v\\ \rho uv\\ \rho v^2+p\\ (E+p)v\end{pmatrix}=0. \tag{4.3}$$

Here, ρ is the density, u and v are the velocity components in x- and y-dimension, p is the pressure, and E is the total energy given by $E=\frac{1}{2}\rho(u^2+v^2)+\frac{p}{\gamma-1}$. Similarly, the time step is evaluated by

$$\Delta t=\frac{CFL}{\max_{i,j}\left(\frac{c_{i,j}+|u_{i,j}|}{\Delta x},\frac{c_{i,j}+|v_{i,j}|}{\Delta y}\right)}$$

with the local sound speed $c_{i,j}=\sqrt{\gamma p_{i,j}/\rho_{i,j}}$.

We solve the Riemann problem for (4.3) with the following initial condition

$$(\rho,u,v,p)(x,y,0)=\begin{cases}(\rho_1,u_1,v_1,p_1), & \text{if } x>0.5, y>0.5,\\ (\rho_2,u_2,v_2,p_2), & \text{if } x<0.5, y>0.5,\\ (\rho_3,u_3,v_3,p_3), & \text{if } x<0.5, y<0.5,\\ (\rho_4,u_4,v_4,p_4), & \text{if } x>0.5, y<0.5.\end{cases}$$

The computational domain is chosen to be $[0,1]\times[0,1]$. According to [10], there are 19 different admissible configurations separated by rarefaction, shock and contact wave. The solutions of all the different configurations are computed on a 400×400 grid and we just show the following two initial data only:

$$\textcircled{1}\begin{cases}(\rho_1,u_1,v_1,p_1)=(0.5313,0,0,0.4),\\(\rho_2,u_2,v_2,p_2)=(1,0.7276,0,1),\\(\rho_3,u_3,v_3,p_3)=(0.8,0,0,1),\\(\rho_4,u_4,v_4,p_4)=(1,0,0.7276,1),\end{cases}$$

$$\textcircled{2}\begin{cases}(\rho_1,u_1,v_1,p_1)=(1,0,0.3,1),\\(\rho_2,u_2,v_2,p_2)=(2,0,-0.3,1),\\(\rho_3,u_3,v_3,p_3)=(1.0625,0,0.2145,0.4),\\(\rho_4,u_4,v_4,p_4)=(0.5197,0,-0.4259,0.4).\end{cases}$$

For initial data ①, the exact solution consists of two shocks and two contact waves. For initial data ②, the exact solution contains one shock, one rarefaction and two contact waves. The density contour lines subject to the above two initial conditions are shown in Fig.4. From these figures, we notice that SD4 computes the wave structures correctly and gives similar resolutions of discontinuities as in [10]. Especially, the proposed scheme avoids the intricate and time-consuming calculations of the specific problems' eigensystem in contrast to upwind schemes.

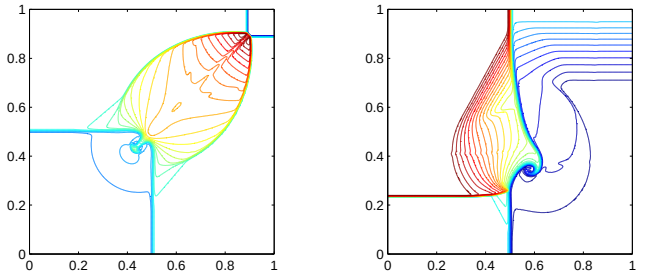

(a) Initial data ① with T=0.25 (b) Initial data ② with T=0.3

Figure 4. Contour plots of the density

5. Conclusion

In this work, we have developed a high order semi-disctete central-upwind scheme for solving nonlinear hyperbolic conservation laws. The new scheme can be seen as a modification of Peer's central scheme. The main technique here is the use of more precise information of the local propagation speeds. We also generalize the proposed scheme for the computations in two-dimensional case. The resulting scheme is still free of Riemann-solver. What's more, it is based on non-staggered grids and therefore our scheme is very simple to be implemented, especially in multidimensional case. In numerical experiments, the scheme is compared to CNO4-N scheme, which is another non-staggered version of Peer's scheme, and it is observed that our scheme has a better accuracy and resolution with less computational time.

References

[1] M. Castro, B. Costa, and W. S. Don, *High order weighted essentially non-oscillatory WENO-Z schemes for hyperbolic conservation laws*, J. Comput.

Phys., 230(2011), 1766–1792.

[2] L. Cai, W. X. Xie, Y. F. Nie, and J. H. Feng, *High-resolution semi-discrete hermite central-upwind scheme for multidimensional Hamilton–Jacobi equations*, Appl. Numer. Math., 80(2014), 22–45.

[3] M. Dehghan and R. Jazlanian, *A high-order non-oscillatory central scheme with non-staggered grids for hyperbolic conservation laws*, Comput. Phys. Commun., 182(2011), 1284–1294.

[4] Y. M. Hu, J. Z. Chen and J. H. Feng, *A fifth-order semi-discrete central-upwind scheme for hyperbolic conservation laws*, Chinese Journal of Computational Physics, 25(2008), 29–35 (in Chinese).

[5] A. Harten, B. Engquist, S. Osher, and S. R. Chakravarthy, *Uniformly high order accurate essentially non-oscillatory schemes, III*, J. Comput. Phys., 71(1987), 231–303.

[6] G. S. Jiang and C. W. Shu, *Efficient implementation of weighted ENO schemes*, J. Comput. Phys., 126(1996), 202–228.

[7] A. Kurganov and D. Levy, *A third-order semidiscrete central scheme for conservation laws and convection-diffusion equations*, SIAM J. Sci. Comput., 22(2000), 1461–1488.

[8] A. Kurganov, S. Noelle, and G. Petrova, *Semidiscrete central-upwind schemes for hyperbolic conservation laws and Hamilton-Jacobi equations*, SIAM J. Sci. Comput., 23(2001), 707–740.

[9] A. Kurganov and G. Petrova, *A third-order semi-discrete genuinely multidimensional central scheme for hyperbolic conservation laws and related problems*, Numer. Math., 88(2001), 683–729.

[10] P. D. Lax and X. D. Liu, *Solution of two-dimensional Riemann problems of gas dynamics by positive schemes*, SIAM J. Sci. Comput., 19(1998), 319–340.

[11] D. Levy, G. Puppo, and G. Russo, *Central WENO schemes for hyperbolic systems of conservation laws*, M2NA Math. Model. Numer. Anal., 33(1999), 547–571.

[12] D. Levy, G. Puppo, and G. Russo, *Compact central WENO schemes for multidimensional conservation laws*, SIAM J. Sci. Comput., 22(2000), 656–672.

[13] H. Nessyahu and E. Tadmor, *Non-oscillatory central differencing for hyperbolic conservation-laws*, J. Comput. Phys., 87(1990), 408–463.

[14] A. A. I. Peer, A. Gopaul, M. Z. Dauhoo, and A. Bhuruth, *A new fourth-order non-oscillatory central scheme for hyperbolic conservation laws*, Appl. Numer. Math., 58(2008), 674–688.

[15] C.-W. Shu, *High order weighted essentially nonoscillatory schemes for convection dominated problems*, SIAM Rev., 51(2009), 82–126.

[16] S. Serna and A. Marquina, *Power ENO methods: a fifth-order accurate weighted Power ENO method*, J. Comput. Phys., 194(2004), 632–658.

[17] Y. H. Zahran, *Non-oscillatory central-upwind scheme for hyperbolic conservation laws*, Int. J. Comput. Fluid Dyn., 21(2007), 11–19.